Scientific Papers. Series E. Land Reclamation, Earth Observation & Surveying, Environmental Engineering. Vol. XIV, 2025
Print ISSN 2285-6064, CD-ROM ISSN 2285-6072, Online ISSN 2393-5138, ISSN-L 2285-6064

NUMERICAL STUDY OF THE CYLINDRICAL SHAFT'S BEHAVIOUR USING 3D FINITE ELEMENT METHOD

Elena-Mihaela STAN, Horațiu POPA, Daniel MANOLI

Technical University of Civil Engineering of Bucharest,
122-124 Lacul Tei Blvd, District 2, Bucharest, Romania

Corresponding author email: elena-mihaela.stan@phd.utcb.ro

Abstract

The numerical modelling of the cylindrical shafts can be done using finite element method in axisymmetric or three-dimensional conditions. For this study, the 3D finite element method has been used to analysed the cylindrical shaft's behaviour regarding the earth pressure distribution, the vertical displacements of the soil and the horizontal displacements of the diaphragm wall. Thus, a parametric study has been carried out in which the cylindrical shafts radius, the length of the diaphragm wall and the excavation depth have been varied. For all the numerical models, the cohesive and cohesionless soil has been used. The results show the influence of all these parameters on the retaining walls' behaviour. Also, the influence of the soil type is explained.

Key words*: 3D finite element method, cylindrical shafts, lateral displacements, excavation.*

INTRODUCTION

Cylindrical shafts are used for specific constructions like pumping stations, tunnel access, underground parkings, launch points for the TBM, tunnel ventilation systems. Due to these specific functionalities and their shape, there is limited information regarding the cylindrical shaft's calculation methods and their behaviour. It is necessary to determine the earth pressure acting on the retaining wall and its lateral displacements. The classical earth pressure theories can be successfully used under plane strain conditions, but, in the case of cylindrical shafts, due to the arching effect developed around the retaining wall, these theories have to be updated.

The first studies regarding the earth's pressure distribution on cylindrical shafts were performed by (Westergaard, 1940) and later on improved by (Terzaghi, 1943). They have shown that the lateral earth pressure increases with depth and reaches a constant value. (Prater, 1977) consider that the lateral earth pressure is increasing up to a maximum value and then is decreasing until reaching a zero value at a depth equal to 8.5 of the excavation's radius.

There is a solid correlation between the lateral earth pressure distribution determined using physical modelling of cylindrical shafts and the one calculated using Terzaghi's theory (Tobar & Meguid, 2011). Also, the results obtained using finite element method are in good agreement with the one determined using physical modelling. The lateral displacements of the retaining wall increase with depth up to a maximum value which is located above the final excavation surface (Tangjarusrutaratorn et al., 2022).

Based on the measured vertical and horizontal displacements obtained from the centrifuge tests and in situ works, equations that can be used to calculate the vertical and horizontal displacements have been developed (New & Bowers, 1994; Le et al., 2019). Generally, these equations do not take into account the shaft diameter and the soil parameters and use empirical coefficients. Schwamb and Soga, (2015), made a comparison between multiple field measurements of the ground settlement and the equation propose by (New & Bowers, 1994). They have shown that the measured ground settlements are smaller than those calculated using the proposed equation and that the results are influenced by the shaft diameter. Schwamb and Soga, (2015), also performed a series of numerical back-analysis carried out using the finite element method in 2D axisymmetric conditions. They analysed the influence of different parameters such as diaphragm wall

thickness, wall stiffness and anisotropy, soil models or the diaphragm wall installation type. The results shown that the thickness of the diaphragm wall has a slightly effect on the wall deflections. The field data are in good agreement with the results of the analysis of an isotropic wall, while the analysis of an anisotropic wall overestimated the wall deflections indicating that the diaphragm wall behaved isotropically despite the joints between the diaphragm wall's panels. Assuming a wished-in-place wall is a reasonable simplification compared to modelling the diaphragm wall installation.

The finite element method (FEM) is a common calculation method used in geotechnical engineering which allows the soil-structure interaction modelling and requires to use complex constitutive models for describing the soil behaviour. One of these complex constitutive models is hardening soil model (HSM), which is used for this paper purpose also.

The circular shafts can be modelled using the finite element method in 2D axisymmetric or 3D conditions. This paper presents the results of a parametric study which has been conducted using the 3D finite element method.

MATERIALS AND METHODS

For this study, the 3D finite element method has been used to analyse the cylindrical shaft behaviour in terms of lateral earth pressure, displacements of the soil and of the retaining wall. The design software used for numerical modelling was Plaxis 3D.

A parametric study has been carried out in which the cylindrical shafts radius (r), the excavation depth (H) and the length of the diaphragm wall (L) have been varied. The excavation depth has values between 10 and 50 m and the length of the diaphragm wall was given values ranging from the excavation depth plus one meter to double of the excavation depth. Generally, the shafts radius has values between 10 and 500 m. For the 10 m deep excavation and the 20 m long diaphragm wall, the excavation radius ranges between 10 and 1000 m.

Generally, the soil parameters must be chosen based on the geotechnical study carried out on the analysed site. There are multiple methods of computing the characteristic values of the soil parameters, including the shearing resistance parameters (Olinic, 2014).

For the purpose of this study, the soil parameters have been chosen based on previous experience for two common soil types. Thus, for all the numerical models, the cohesive and cohesionless soil have been used.

The parameters for the two types of soil are shown in Table 1. For this study, the hardening soil model has been used. Totally, a number of 1392 numerical models have been carried out. Due to the large number of numerical models, Python 3.11.5 was employed to facilitate their calculus.

Table 1. Soil parameters used in the numerical analysis

Soil type	γ	γ_{sat}	E_{50}^{ref}	E_{oed}^{ref}	E_{ur}^{ref}	ν_{ur}	m	c'	ϕ'	R_{inter}
	[kN/m^3]	[kN/m^3]	[kPa]	[kPa]	[kPa]	[-]	[-]	[kPa]	[kPa]	[-]
Cohesionless	19.5	20.50	25000	25000	75000	0.30	0.5	5	30	0.67
Cohesive	19.5	20.50	15000	15000	45000	0.35	0.6	40	15	0.67

γ - unit weight; γ_{sat} - saturated unit weight; E_{50}^{ref} - secant stiffness in standard drained triaxial test; E_{oed}^{ref} - tangent stiffness for primary oedometer loading; E_{ur}^{ref} - unloading/reloading stiffness; ν_{ur} - Poisson's ratio for unloading-reloading; m - power for stress-level dependency of stiffness; c' - effective cohesion; ϕ' - Effective angle of internal friction; R_{inter} - strength reduction factor.

The diaphragm wall is modelled as a plate and the capping beam is defined as a beam element. For both, the linear elastic constitutive model has been used. The material properties are shown in Tables 2 and 3.

The dimensions of the numerical model are chosen according to the excavation depth: the model is extended to 5 times the excavation depth upstream of the retaining wall and 3 times below the excavation surface (Figure 1).

Table 2. Material properties of the diaphragm wall

Material	γ	E_1	ν_{12}	d
	[kN/m^3]	[kPa]	[-]	[m]
Concrete	25	3.10e7	0.2	0.45

Table 3. Material properties of the capping beam

Material	γ	E	height	width
	[kN/m^3]	[kPa]	[m]	[m]
Concrete	25	3.10e7	0.60	0.45

Regarding the model boundaries, the bottom boundary is fixed in all directions and the vertical boundaries are fixed on horizontal directions and free on vertical direction.

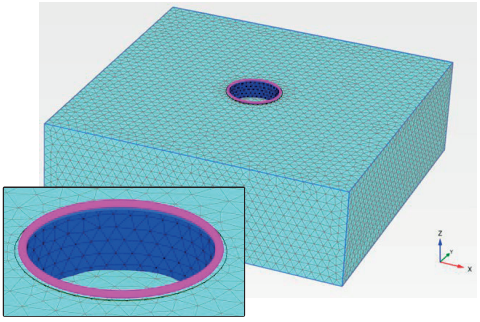

Figure 1. Numerical model – mesh generation

In order to perform finite element calculations, the numerical model has to be divided into finite elements. The relative element size of 0.02 has been chosen.

RESULTS AND DISCUSSIONS

The lateral earth pressure

Figure 2 show the lateral earth pressure diagrams acting on the retaining wall of a 10 m depth circular excavation (H), with 20 m wall length and 0.45 m wall thickness, in cohesionless soil. The excavation radius ranges between 10 and 100 m. Also, the active (γHk_a) and at rest (γHk_0) earth pressure diagrams are plotted.

The at-rest earth pressure coefficient has been calculated using the Jaky empirical relationship, $k_0 = 1 - \sin(\varphi)$, the same relationship used by Plaxis 3D, for both types of soil. Figure 3 shows the lateral earth pressure diagrams acting on the retaining structure with the same geometric parameters as in the Figure 2, but in the case of the cohesive soil.

The results obtained using FEM do not correspond to the ones obtained using the analytical solutions presented in the first section of this paper. Generally, the lateral earth pressure has values between the active and at rest earth pressure. Also, the lateral earth pressure varies approximatively linearly with depth.

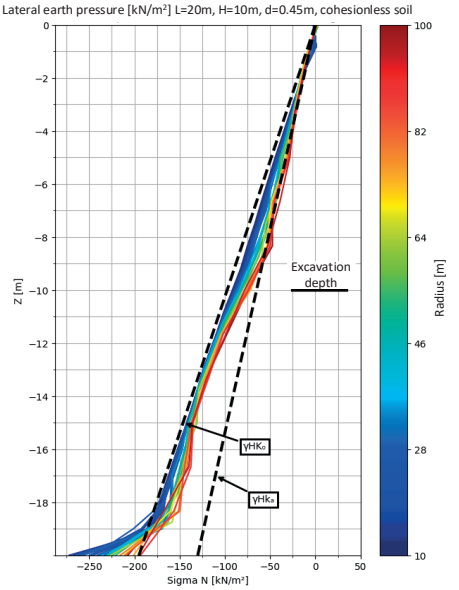

Figure 2. The lateral earth pressure diagrams for a circular excavation with H = 10 m, L = 20 m and r = 10÷100 m, cohesionless soil

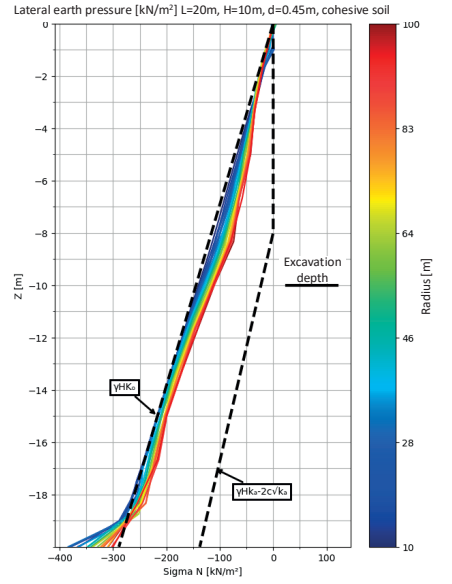

Figure 3. The lateral earth pressure diagrams for a circular excavation with H = 10 m, L = 20 m and r = 10÷100 m, cohesive soil

In the case of the cohesionless soil, for small values of the radius, the lateral earth pressure has values close to those of the at rest earth pressure. For larger values of the radius, the lateral earth pressure diagrams no longer vary linearly with depth. Also, at the final excavation depth, the values of the lateral earth pressure decrease to values lower than that of the active earth pressure. In the case of cohesive soil (Figure 3), the earth pressure variation with increasing radius is smaller and its values are close to those of the at rest earth pressure.

Horizontal displacements of the retaining structure

Figure 4 and Figure 5 show the lateral displacements diagram of the retaining wall of a 10m depth circular excavation (H), with 20 m wall length and 0.45 m wall thickness, in cohesionless soil. The excavation radius varies between 10 and 250 m (Figure 4) and between 10 and 1000 m (Figure 5).

Figure 5 shows also the lateral displacements diagram for a plane strain calculus of an excavation with the same characteristics.

For cylindrical shafts, the maximum value of the horizontal displacement of the retaining wall is located above the final excavation depth, due to the arching effect.

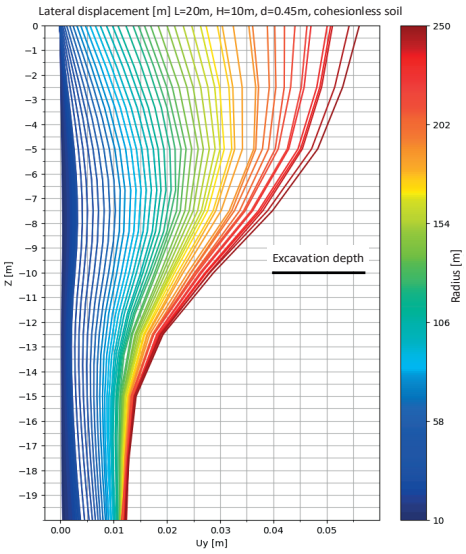

Figure 4. The lateral displacement diagram of the retaining wall, for a circular excavation with H = 10 m, L = 20 m and r = 10÷250 m, cohesionless soil

For a radius greater than 200 m, the shape of the lateral displacement diagram changes, the maximum value being located at the upper part of the retaining wall. This behaviour is specific to the plane strain conditions.

However, even for large radii up to 1000 m, the maximum value of the horizontal displacement is smaller than that obtained from the plane strain calculus, further indicating the presence of the arching effect.

The maximum horizontal displacement increases with increasing radius and excavation depth. For the same excavation depth, the variation of the maximum horizontal displacement with the radius is showing a trend.

Figure 6 and Figure 7 show the variation of the maximum horizontal displacement normalized with the excavation depth with the radius, for cohesionless and cohesive soil, for radius smaller than 100 m.

For each type of soil and each excavation depth, these variations show a similar trend and the differences between them are slight.

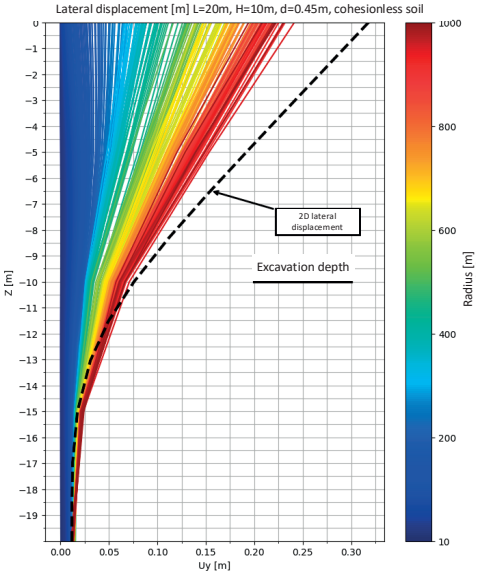

Figure 5. The lateral displacement of the retaining wall's diagram, for a circular excavation with H = 10 m, L = 20 m and r = 10÷1000 m, cohesionless soil

In order to found a function that can be used to approximate the maximum horizontal displacement depending on the excavation depth, on the type of soil and on the radius, for

each graph, the median values of the maximum horizontal displacements have been calculated and plotted on the graph.

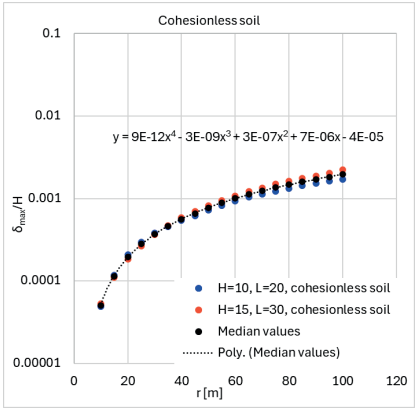

Figure 6. Variation of the maximum horizontal displacement normalized with the excavation depth, with the radius, r≤100 m, cohesionless soil

For these median values, a fourth-degree polynomial function has been determined. The resulted functions for each type of soil are presented below.

For cohesionless soil, the radii between 10 and 100 m and excavation depths between 10 and 15 m, the maximum horizontal displacement can be approximated with the following function:

$$\frac{\delta_{max}}{H} = 8.84E-12 \cdot r^4 - 2.54E-9 \cdot r^3 + 2.89E-7 \cdot r^2 + 6.70E-6 \cdot r - 4.26E-5$$

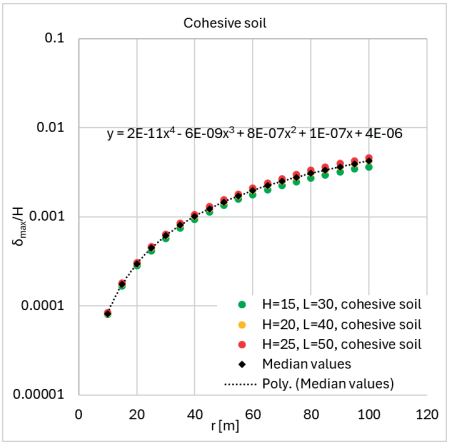

Figure 7. Variation of the maximum horizontal displacement normalized with the excavation depth, with the radius, r≤100 m, cohesive soil

For cohesive soil, the radii between 10 and 100 m and excavation depths between 15 and 25 m, the maximum horizontal displacement can pe approximate with the following function:

$$\frac{\delta_{max}}{H} = 1.81E-11 \cdot r^4 - 5.96E-9 \cdot r^3 + 8.39E-7 \cdot r^2 + 1.19E-7 \cdot r - 3.97E-6$$

The differences between the calculated and the approximated horizontal displacements are, generally, smaller than 10% and maximum 16% for radii greater than 60 m.

The maximum value of the horizontal displacement of the retaining wall is located above the final excavation level (Figure 8). For the same excavation depth, the maximum horizontal displacements occur at the same depth for both cohesive and cohesionless soil types.

For excavation depths smaller than 20 m, the maximum horizontal displacement with respect to the final excavation depth, is encountered for a ratio $z/H = (0.66 \div 0.86)$.

For excavation depths greater than 25 m, the maximum horizontal displacement with respect to the final excavation depth, is encountered for a ratio $z/H = (0.75 \div 0.93)$.

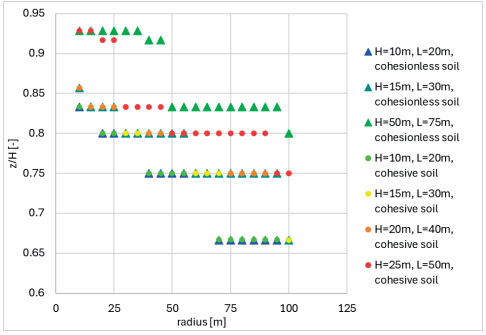

Figure 8. Depth at which the maximum horizontal displacement (z) occurs, normalized with the final excavation depth (H), depending on the radius, excavation depth and soil type

As the radius increases, the depth at which the maximum horizontal displacement occurs decreases but cannot be expressed as a function.

Vertical displacements of the ground behind the retaining structure

Considering the shape of the horizontal displacement diagram and its values at the top of

the wall, it is expected that the vertical displacement of the ground behind the retaining structure will swell in its immediate vicinity and then will start to settle at a certain distance away from the retaining wall. This behaviour is highlighted in Figures 9 and 10.

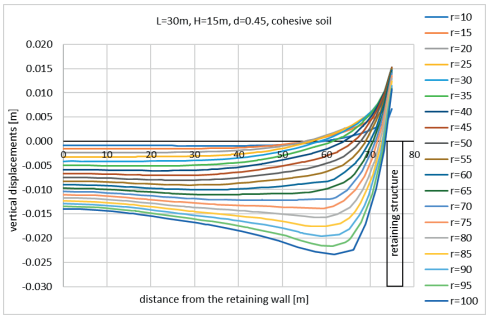

Figure 9. The vertical displacements of the ground behind the retaining wall, for a circular excavation with H = 15 m, L = 30 m and r = 10÷100 m, cohesive soil

The maximum vertical displacements for cylindrical shafts modelled in cohesive soil are greater than those obtained for circular excavation executed in cohesionless soil.

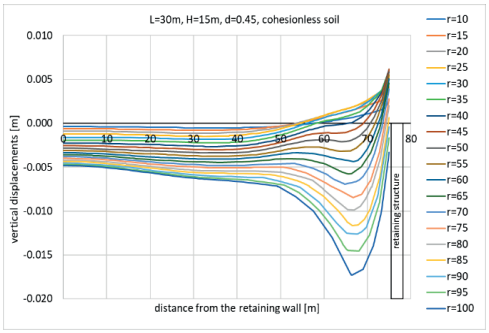

Figure 10. The vertical displacements of the ground behind the retaining wall, for a circular excavation with H = 15 m, L = 30 m and r = 10÷100 m, cohesionless soil

Depending on the type of soil and the radius, the maximum values of the vertical displacement of the soil occurs at different distance from the retaining wall. For small values of the circular excavation radius, the maximum vertical displacement occurs at a large distance from the retaining wall, between $(2 \div 5)H$, the ratio increasing with the excavation depth.

For large values of the circular excavation radius, the maximum vertical displacement occurs at a smaller distance from the retaining wall, between $(0.45 \div 1.40)H$, the ratio increasing with the excavation depth (Figure 11).

Figure 12 shows the relationship between the maximum vertical displacements (s_{max}) and the maximum horizontal displacements (δ_{max}), normalized with the excavation depth (H), for different excavation depths and circular excavation radii.

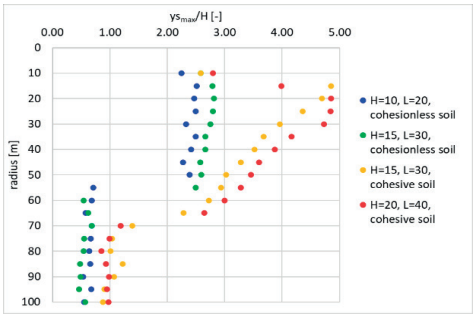

Figure 11. The distance at which the maximum vertical displacements occur from the retaining wall, normalized by the excavation depth (ys_{max}/H), for different excavation depths, depending on the circular excavation radius

The maximum vertical displacements are not equal to the maximum horizontal displacements, but there is the following relationship between them:

$$s_{max} = \frac{\delta_{max}}{2} \div \frac{\delta_{max}}{4}$$

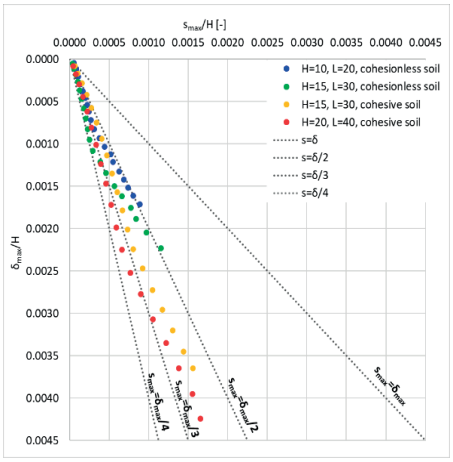

Figure 12. The dependence between the maximum vertical displacements (s_{max}) and maximum horizontal displacements (δ_{max}), normalized by the excavation depth (H), for different excavation depth and excavation radius

CONCLUSIONS

This paper presents a parametric study regarding the cylindrical shaft behaviour, in which the radius, the length of the diaphragm wall and the excavation depth have been varied. Also, two types of soil have been used: cohesionless and cohesive.

For this parametric study, the finite element method has been used to perform the numerical modelling and calculus.

The results show the lateral earth pressure acting on the retaining wall and its comparison with the at-rest and active earth pressure diagrams. Thus, for common shafts radii smaller than 100 m, the lateral earth pressure acting on the retaining wall varies approximatively linearly with depth and has values close to those of the at rest earth pressure.

For each type of soil, relationships that can be used to approximate the maximum horizontal displacement depending on the excavation depth, on the type of soil and on the radius were proposed.

However, these relationships are limited for a small interval of excavation depths and cannot be applied to a mixed stratigraphy.

Generally, in the immediate vicinity of the retaining structure, the vertical displacements of the ground swell. For small values of the shaft radius, the maximum vertical displacement occurs at a large distance from the retaining wall.

For large values of the circular excavation radius, the maximum vertical displacement occurs at a smaller distance from the retaining wall.

The ratio between the maximum vertical and horizontal displacements is not equal to one, as proposed in the technical literature.

REFERENCES

Le, B.T., Goodey, R.J., & Divall, S. (2019). Subsurface ground movements due to circular shaft construction. *Soils and Foundations, 59,* 1160-1171.

New, B.M., & Bowers, K.H. (1994). Ground movement model validation at the Heathrow Express trial tunnel. *Tunelling'94,* 301-329.

Olinic, E. (2014). The influence of geotechnical investigations magnitude on characteristic values of soils parameters. *International Multidisciplinary Scientific GeoConference: SGEM: Surveying Geology & Mining Ecology Management, 2,* 915-920.

Prater, E.G. (1977). An examination of some theories of earth pressure on shaft linings. *Canadian Geotechnical Journal*, *14*(1), 91–106.

Schwamb, T. & Soga, K. (2015). Numerical modelling of a deep circular excavation at Abbey Mills in London. *Geotechnique, 65*(7), 604-619.

Tangjarusrutaratorn, T., Miyazaki, Y., Sawamura, Y., Kishida, K., & Kimura, M. (2022). Numerical investigation on arching effect surrounding deep cylindrical shaft during excavation process. *Underground space, 7*(5), 944–965.

Terzaghi, K. (1943). *Theoretical Soil Mechanics*. New York: John Wiley and Sons.

Tobar, T., & Meguid, M.A. (2011). Experimental Study of the Earth Pressure Distribution on Cylindrical Shafts. *Journal of geotechnical and geoenvironmental engineering, 137*(11), 1121-1125.

Westergaard, H.M. (1940). Plastic state of stress around a deep well. *Journal of the Boston Society of Civil Engineers*, *27*(1), 387–391.